ACCOUNTS of chemical research

Article

Cite This: Acc. Chem. Res. 2019, 52, 1006−1015

pubs.acs.org/accounts

The Surface of Ice under Equilibrium and Nonequilibrium Conditions

Yuki Nagata,[†] Tetsuya Hama,[‡] Ellen H. G. Backus,[†,§] Markus Mezger,[†,∥] Daniel Bonn,[⊥] Mischa Bonn,[*,†] and Gen Sazaki[*,‡]

[†]Max Planck Institute for Polymer Research, Ackermannweg 10, 55128 Mainz, Germany

[‡]Institute of Low Temperature Science, Hokkaido University, Sapporo 060-0819, Japan

[§]Department of Physical Chemistry, University of Vienna, Waehringer Strasse 42, 1090 Vienna, Austria

[∥]Institute of Physics, Johannes Gutenberg University Mainz, 55128 Mainz, Germany

[⊥]Van der Waals-Zeeman Institute, University of Amsterdam, Science Park 904, 1098 XH Amsterdam, The Netherlands

CONSPECTUS: The ice premelt, often called the quasi-liquid layer (QLL), is key for the lubrication of ice, gas uptake by ice, and growth of aerosols. Despite its apparent importance, in-depth understanding of the ice premelt from the microscopic to the macroscopic scale has not been gained. By reviewing data obtained using molecular dynamics (MD) simulations, sum-frequency generation (SFG) spectroscopy, and laser confocal differential interference contrast microscopy (LCM-DIM), we provide a unified view of the experimentally observed variation in quasi-liquid (QL) states. In particular, we disentangle three distinct types of QL states of disordered layers, QL-droplet, and QL-film and discuss their nature. The topmost ice layer is energetically unstable, as the topmost interfacial H_2O molecules lose a hydrogen bonding partner, generating a disordered layer at the ice−air interface. This disordered layer is homogeneously distributed over the ice surface. The nature of the disordered layer changes over a wide temperature range from −90 °C to the bulk melting point. Combined MD simulations and SFG measurements reveal that the topmost ice surface starts to be disordered around −90 °C through a process that the topmost water molecules with three hydrogen bonds convert to a doubly hydrogen-bonded species. When the temperature is further increased, the second layer starts to become disordered at around −16 °C. This disordering occurs not in a gradual manner, but in a bilayer-by-bilayer manner.

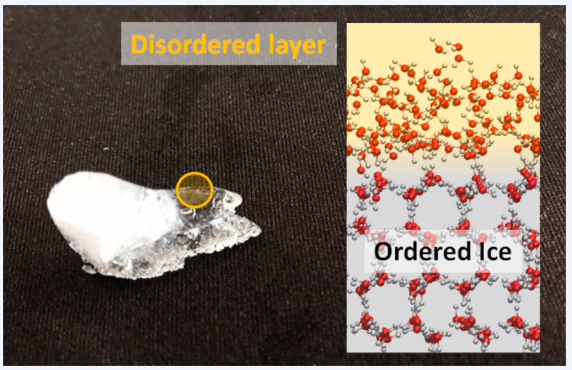

When the temperature reaches −2 °C, more complicated structures, QL-droplet and QL-film, emerge on the top of the ice surface. These QL-droplets and QL-films are inhomogeneously distributed, in contrast to the disordered layer. We show that these QL-droplet and QL-film emerge only under supersaturated/undersaturated vapor pressure conditions, as partial and pseudopartial wetting states, respectively. Experiments with precisely controlled pressure show that, near the water vapor pressure at the vapor-ice equilibrium condition, no QL-droplet and QL-film can be observed, implying that the QL-droplet and QL-film emerge exclusively under nonequilibrium conditions, as opposed to the disordered layers formed under equilibrium conditions.

These findings are connected with many phenomena related to the ice surface. For example, we explain how the disordering of the topmost ice surface governs the slipperiness of the ice surface, allowing for ice skating. Further focus is on the gas uptake mechanism on the ice surface. Finally, we note the unresolved questions and future challenges regarding the ice premelt.

INTRODUCTION

The ice premelt is the disordering of water molecules at the ice surface. It is commonly referred to as a quasi-liquid layer (QLL).[1,2] After Faraday's postulation of the presence of the ice premelt, it has been identified as being important for various physical phenomena. For instance, the ice premelt is crucial for reducing the friction on ice,[3] nucleating aerosols, and providing a unique platform for atmospheric reactions on ice.[4] Despite many experimental and theoretical attempts to characterize the ice premelt definitively, the conclusions regarding its thickness and nature vary substantially.[5,45] It is still unclear whether the QLL on top of ice surfaces as identified by different methods all represent the same kind of water layer. For example, the thickness of the QLL has been inferred from X-ray scattering, atomic force microscopy, ellipsometry, electron diffraction, and molecular dynamics (MD) simulations.[1,5,6] These individual techniques may probe different observables, resulting in different QLL thicknesses. Furthermore, when the temperature is close to the melting point, the vapor pressure starts to affect

Received: December 3, 2018
Published: March 29, 2019

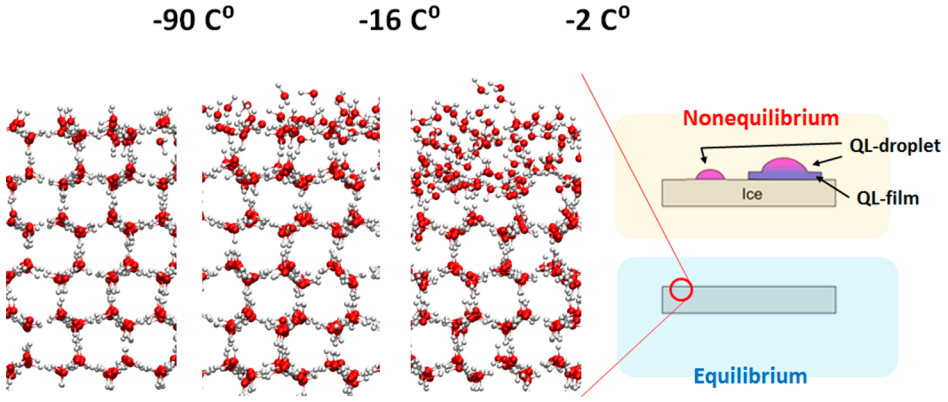

Figure 1. Variation of the ice surface structures at the basal face. Above −90 °C (−16 °C), the first (the second) bilayer becomes mobile. Above −2 °C in nonequilibrium conditions, the partial and pseudopartial wetting states emerge. The structures of ice surfaces are generated from the MD trajectories at −103, −73, and −13 °C of refs 14 and 15.

the molecular organization at the ice surface critically, making the identification of the QLL difficult. As such, characterizing the QLL on the ice surface has been a challenge.

So far, at least three different quasi-liquid (QL) states have been identified on the ice surface under equilibrium and nonequilibrium conditions, which are schematically displayed in Figure 1. A disordered layer starts to be formed above −90 °C.[1,7,8] This disordered layer arises from the energetically unstable topmost water molecules due to the interruption of the hydrogen bonding at the topmost ice layer and is thus homogeneously distributed over the ice surface at the equilibrium condition, as the hydrogen bonding is interrupted everywhere on the ice surface. The water molecules in this layer is mobile[9] and its viscosity has been reported to be comparable to that of bulk water.[10] This disordered layer is typically captured by using MD simulations and molecular-scale measurements such as sum-frequency generation (SFG) spectroscopy.

When the temperature approaches the bulk melting point, two additional QL states, QL-droplets and QL-films, emerge, but likely only under conditions deviating from the vapor-ice equilibrium.[11] These droplets and films are inhomogeneously distributed in space on the ice surface, and have been reported to be 20 and 200 times more viscous than bulk water.[12] The QL-droplet and QL-film are typically observed using confocal microscopy techniques. The confocal microscopy observations indicate that the QL-droplet and QL-film appear not only on the basal face but also on the prism faces and high-index faces above −2 °C,[13] while in the temperature range from −90 to −2 °C, only one QL state, disordered layer, exists.

In this Account, we review the literature in which the ice premelt is characterized with different tools, MD simulation, SFG spectroscopy and laser confocal differential interference contrast microscopy (LCM-DIM), at different vapor pressures and temperatures. Furthermore, we explain how heterogeneous the ice melting is by examining the deviations between the experimental/simulation data on the ice surfaces and the predictions from the continuum model. Finally, we summarize the unsolved questions and future challenges for understanding the premelting of ice.

Continuum Model of Ice Surface Melting

Surface-induced premelting is a phenomenon found for a wide class of materials, not only at ice surfaces but also in metals, rare gases, and organic substances.[16] In the framework of classical equilibrium thermodynamics, surface-induced premelting can be described as wetting transition, where the crystal is wetted by its own melt. The free energy $F(d)$ of the system is described as a function of the QLL thickness d. Negative $\Delta F(d) = F(d) - F(d = 0)$ indicates that the surface can melt before the bulk; a QLL is formed at the surface of a crystalline solid below the bulk melting point T_m, when the temperature T is above the onset temperature T_0(Figure 2A and B).

Considering a three-layer system (crystal, QLL, vapor), the free energy $F(d)$ per surface area A is given by[17]

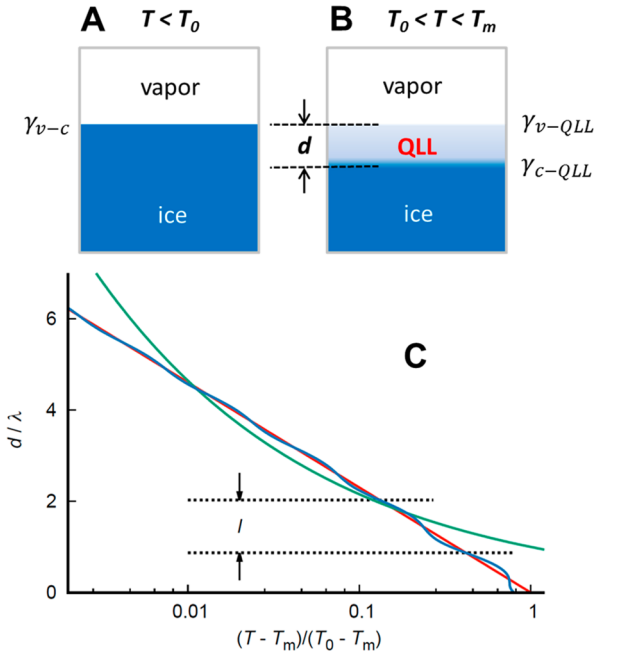

Figure 2. (A) Crystal−vapor interface below the onset temperature and (B) surface-induced premelting above the onset temperature. (C) Temperature variation of normalized growth law $d(T)/\lambda$ governed by short-range repulsive (red, eq 3) and long-range van der Waals interactions (green, eq 4). Structural forces can lead to so-called layer-by-layer melting where discrete equidistant oscillations of thickness l are observed in $d(T)$ (blue).

DOI: 10.1021/acs.accounts.8b00615
Acc. Chem. Res. 2019, 52, 1006−1015

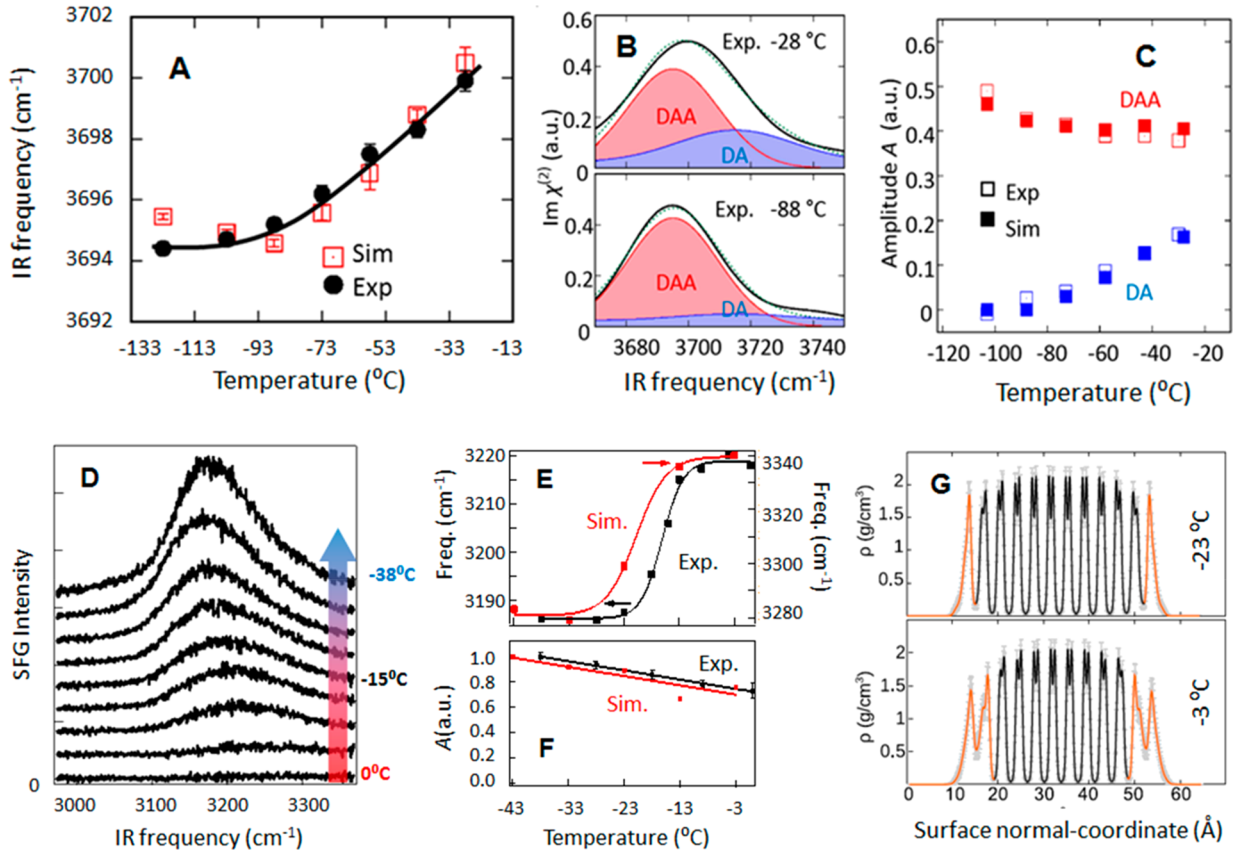

Figure 3. (A) Free O−H stretch peak frequency vs temperature. The lines are to guide the eye. Reproduced with permission from ref 15. Copyright 2017 American Physical Society. (B) Experimentally measured SFG spectra of the free O−H stretch mode (black lines). The contributions from the DAA (red lines) and DA species (blue lines) are obtained from Gaussian fits to the experimental data. The sum of the fit curves for DAA and DA species are depicted in broken lines. (C) Variations of the SFG amplitudes of the DAA and DA contributions. (B, C) Reproduced with permission from ref 9. Copyright 2018 American Chemical Society. (D) SFG spectra in the hydrogen-bonded O−H stretch region for the basal face of ice I_h crystal form. (E) First moment of the frequency distribution of the experimental SFG intensity (left axis) and peak maximum of the simulated SFG spectra (right axis) vs temperature. Sigmoidal fits are added. (F) Observed spectral area under the free O−H SFG peaks. The lines are to guide the eye. (G) Density profiles for the basal planes of ice I_h. (E−G) Molten (orange) vs crystalline (black) layers are marked. Reproduced with permission from ref 23. Copyright 2017 National Academy of Sciences.

$$\frac{F(d)}{A} = \gamma_{v-c} + \varphi(d)\Delta\gamma + d\frac{\Delta H}{V}\frac{T_m - T}{T_m} \quad (1)$$

where $\gamma_{v-c} \equiv F(d=0)/A$ denotes the surface tension of the vapor−crystal interface. The second term represents the costs for forming the vapor−QLL (γ_{v-QLL}) and crystal−QLL (γ_{c-QLL}) interfaces, where $\Delta\gamma = \gamma_{v-QLL} + \gamma_{c-QLL} - \gamma_{v-c}$, and the prefactor $\varphi(d)$ accounts for the coupling between the vapor−QLL and crystal−QLL interfaces in the premelting regime. When the QLL is absent, $\varphi(d=0) = 0$. For sufficiently large QLL thicknesses, the vapor-QLL and crystal-QLL interfaces are decoupled and $\varphi(d \to \infty)$ becomes unity. The last term in eq 1 contains the molar latent heat of fusion (ΔH) and the molar volume (V) of the QLL, that is proportional to the difference in chemical potentials between the QLL and the crystalline phase. At temperatures below the melting point ($T < T_m$), the third term is always positive. To achieve $\Delta F(d) < 0$ in the limit of T being close to T_m, $\Delta\gamma$ has to be negative, because both γ_{v-c} and $\varphi(d)$ are positive. In this case, a stable QLL can form a complete wetting layer.

Under the assumption of exponentially decaying short-ranged forces,

$$\varphi(d) = 1 - \exp(-d(T)/\lambda) \quad (2)$$

one finds a logarithmic growth law,

$$d(T) = \lambda \ln\frac{T_0 - T_m}{T - T_m} \quad (3)$$

where the parameter λ is directly related to the correlation length of the liquid, via the Landau−Ginzburg model for nonordering surface phase transitions.[18] For long-ranged algebraic decays originating from nonretarded van der Waals forces, i.e., a potential that falls off quadratically with distance d, one obtains a power-law dependence:[17]

$$d(T) \propto \left(\frac{T_0 - T_m}{T - T_m}\right)^{1/3} \quad (4)$$

The variations of d with temperature according to eqs 3 and 4 are depicted in Figure 2C.[19]

For QLL thicknesses at molecular length scales, the QLL cannot be treated as a homogeneous medium. On this length scale, liquids exhibit granularity, due to the discrete and finite dimensions of the molecules. This leads to so-called structural forces. They cause oscillatory components with periodicity l in $\varphi(d)$ (see Figure 2C). Often, l is related to the spacing

DOI: 10.1021/acs.accounts.8b00615
Acc. Chem. Res. 2019, 52, 1006−1015

between high-symmetry planes of a corresponding crystalline phase. This oscillatory term can give rise to equidistant steps in the growth law. Here, a question is to which extent such an oscillatory behavior affects the melting behavior of the ice surface (layer-by-layer vs continuous melt). We shall discuss the melt behavior below.

Moreover, by assuming thermodynamic equilibrium, these continuum models cannot predict the formation of the QL states under nonequilibrium conditions. In fact, when the ice surface is in contact with either supersaturated or undersaturated vapor, QL-droplet and QL-film are generated. The resultant structures can qualitatively differ from the disordered layer present under equilibrium conditions.[11] Below, we outline the QL-droplet and QL-film under both equilibrium and nonequilibrium conditions and reveal their lateral inhomogeneity and their changes in the wetting states with varying water vapor pressure.

Topmost Layer Disordering at ∼ −90 °C: Interconversion of DA to DAA Water Molecules

Premelting of the ice crystal surface starts from the disordering of the topmost layer. To probe a structural variation of the topmost interfacial water molecules, an experimental technique with molecular-level spatial resolution is required. Furthermore, surface-sensitivity is needed to detect such a disordered layer. This can be achieved by using SFG spectroscopy technique. In this technique, an infrared laser beam and a visible laser beam are overlapped in space and time on the sample. The resulting reflecting sum frequency light is detected. Due to its selection rules, no SFG is obtained from centrosymmetric media like bulk water and proton disordered bulk ice, making the method surface-sensitive.[20,21] Moreover, an SFG signal is enhanced if the infrared light is in resonance with a molecular vibration, making the technique molecule-specific. For H_2O molecules at the liquid water−air interface, the hydrogen bonded O−H groups have a frequency below 3550 cm^{-1}, while the free O−H groups in the topmost water layer pointing *up* into the air have a frequency of ∼3700 cm^{-1}.[20]

Figure 3A displays the blueshift of the free O−H stretch mode frequency by increasing the temperature above −90 °C. This blueshift with increasing temperature is somewhat surprising, as the free O−H group of water molecules at the liquid water−air interface shows a redshift with increasing temperature,[14] due to the enhanced anharmonicity of the potential. One would expect the same effect to be operative for water molecules at the ice surface, but the observation is counterintuitive. What does this blueshift of the free O−H peak frequency indicate?

A previous infrared study of water clusters showed that two types of water molecules with a free O−H group, i.e., DAA and DA water molecules, have distinct free O−H frequencies of 3695 and 3715 cm^{-1}, respectively.[22] Here, a DA (DAA) water molecule represents a water molecule with one donating and one accepting (one donating and two accepting) hydrogen bonds. The interconversion from the DAA to DA species with increasing temperature can lead to a blueshift of the free O−H peak frequency, as the width of each of the two peaks is larger than their separation. This scenario can explain the frequency shift of the SFG O−H stretch mode with temperature. In fact, the free O−H SFG features can be well fit with two Gaussians located at 3695 and 3715 cm^{-1} (Figure 3B).[9,15]

The variations of the SFG contributions from the DAA and DA water molecules are plotted in Figure 3C. One can see that the free O−H peak is dominated by the DAA contribution at −90 °C, while one-third of the free O−H peak amplitude is contributed by DA molecules at −30 °C. Such interconversion of DAA and DA indicates that the water molecules in the topmost layer break the hydrogen bonds and then the surface molecules become disordered. From Figure 3A, one can conclude that the disordering of the topmost layer starts at ∼ −90 °C. Note that a similar onset temperature of the disordering of the topmost layer was reported previously through polarization dependent SFG.[7] Here, an important finding is that the disordering of the first layer is characterized by the drastic interconversion between DAA and DA-type water molecules due to the temperature change.

Second Bilayer Disordering at ∼ −16 °C: Layer-by-Layer Melting

Upon further increasing the temperature, at a certain point, the second layer will start to melt. As the water molecules in the second layer have no free O−H group, but are hydrogen-bonded, the SFG response of the hydrogen-bonded O−H stretch mode has to be measured to obtain information about the second layer. The hydrogen-bonded O−H stretch mode of ice can be typically seen in the 3100−3350 cm^{-1} frequency domain.[20] Figure 3D shows the spectra for the ice basal face−air interface of single crystalline ice at 235−273 K in a closed cell with equilibrated vapor-pressure.[23] Upon increasing the temperature, the spectral intensity decreases, as the water molecules are disordered due to thermal excitation. Moreover, the peak maximum shifts to higher frequencies upon heating. This frequency shift is quantified by calculating the first moment of the frequency, which is depicted in Figure 3E. Interestingly, the first moment does not gradually shift but shows a rather steep increase of ∼35 cm^{-1} at ∼ −16 °C. Apparently, a transition in the water hydrogen bond structure in the near-surface area occurs at ∼ −16 °C. As the first layer is already molten at these temperatures, the intensity of the free O−H stretch peak centered at ∼3700 cm^{-1} shows only a weak continuous decrease with increasing temperature, as can be seen in Figure 3F. This indicates that the microscopic structure of the outermost surface layer of water is unchanged within this temperature range.

To connect the SFG results with a molecular-level picture, the experimental data are compared to the SFG spectra computed from the MD simulations.[23] The peak frequency for the hydrogen-bonded O−H stretch mode in the simulated SFG spectra is also plotted in Figure 3E. Similar to the experimental data, a relatively sharp transition is observed at ∼ −21 °C, while the intensity of the free O−H (Figure 3F) shows only a moderate reduction with increasing temperature. The simulation therefore reproduces the experimental results. Based on the good agreement of simulated and experimental SFG data, we examined the density profiles computed from the MD trajectory. These are depicted in Figure 3G.[23] At both −23 and −3 °C, the inner part of the slab consists of clear double peaks, which originates from the bilayer structure of ice. However, at −23 °C, the outermost and at −3 °C the two outermost layers are lacking this double peak, indicating that these layers are rather liquid-like instead of ice-like. The stepwise transition observed in the experimental and calculated SFG spectra according to this simulation thus marks the transition from one to two molten bilayers.[23] In contrast, large-

DOI: 10.1021/acs.accounts.8b00615
Acc. Chem. Res. 2019, 52, 1006−1015

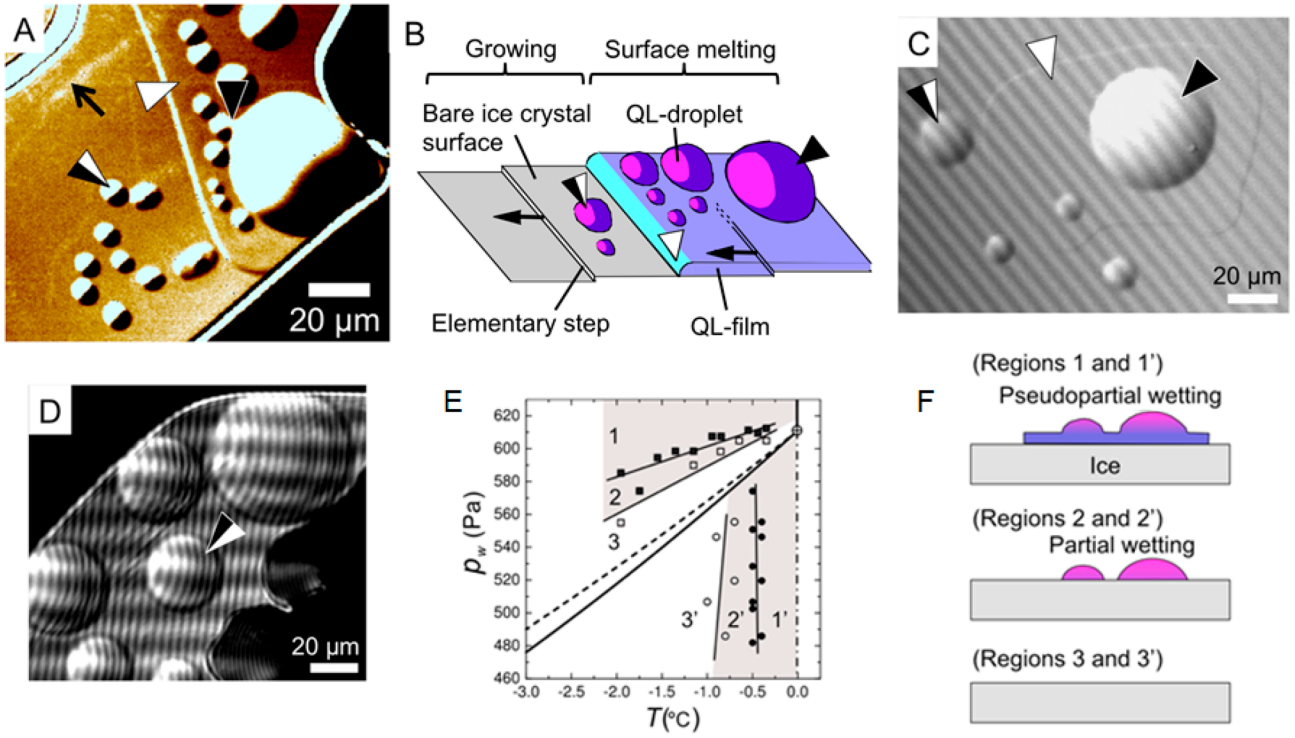

Figure 4. (A) LCM-DIM image of an ice basal face. (B) Schematic illustration. (C,D) Interferometry images of ice basal faces: (C) QL-droplets and a QL-film coexisting; (D) QL-droplets only. Black arrows indicate elementary steps (growing ends of ubiquitous molecular layers, 0.37 nm in thickness) and their growth directions. White arrowheads indicate QL-films on bare ice surfaces. Black/white and black arrowheads point at QL-droplets located on bare ice surfaces and on QL-films, respectively. (A, B) Reproduced with permission from ref 11. Copyright 2012 National Academy of Sciences. (C, D) Reproduced with permission from ref 31. Copyright 2016 National Academy of Sciences. (E) Pressure−temperature diagram for QL-droplet and QL-film. Open squares (circles) indicate critical water vapor pressures (temperatures) above which QL-droplets emerge. Solid squares (circles) indicate critical water vapor pressures (temperatures) above which QL-films emerge. Solid and dotted lines represent the vapor-ice and vapor−liquid water equilibrium curves, respectively. Reproduced with permission from refs 31 and 32 Copyright 2016 National Academy of Sciences. (F) Schematic illustrations of the QL-droplet and QL-film in the different pressure−temperature regions.

scale MD simulations with the coarse-grained water model reveal that the fraction of liquid in the outermost layer of ice increases from ∼0.4 at 250 K to 0.65 at 270 K, while also a small fraction of the second layer is already molten.[24,25] If this is true, the observed frequency shift in the SFG experiment may then be attributed to an increase in the average coordination among liquid-like water molecules in the incomplete layer.[24] The presence/absence of the transition seems thus sensitive to the simulation length and the models of water used for the simulation.[24,26] Further research using accurate all-atom models in a large simulation cell and extended simulation times of a few microseconds would be able to address this controversy.

Emergence of QL-Droplets and QL-Films above −2 °C under Nonequilibrium Conditions

When we further increase the temperature and reach −2 °C, it is known that the QL-droplet emerges.[27] So far, it was believed that this QL-droplet stands on a homogeneously distributed disordered layer.[27] However, by using a recently developed microscopy technique, we have revealed that the QL-droplet emerges not only on the bare ice surface but also on the QL-film. Here, we overview the structure of the ice surface when a QL-droplet emerges, and the vapor pressure condition to generate a QL-droplet.

To visualize ice crystal surfaces with sufficient spatial and temporal resolution, we have combined laser confocal microscopy (LCM) with differential interference contrast microscopy (DIM).[28] LCM has a strong noise reduction function, while DIM provides three-dimensional contrast, with the ability to resolve small height differences. The combination of these techniques allows us to observe individual elementary steps on ice crystal surfaces.[29] Figure 4A is a typical LCM-DIM image of surface melting processes occurring on ice basal faces,[11] demonstrating that LCM-DIM can capture subnanometer features on the ice surface. The image shows, for the first time, that a QL-film with a constant thickness (9 nm)[12] is distributed inhomogeneously in space, in addition to the QL-droplet distributed also inhomogeneously (Figure 4B).

How can these QL-droplet and QL-film states with different morphologies emerge on ice crystal surfaces? In Figure 4A, we observe QL-droplets on a bare ice surface (indicated by a black/white arrowhead) and QL-droplets on a QL-film (indicated by a black arrowhead). From the viewpoint of wetting, the former and the latter correspond to the partial wetting state and the pseudopartial wetting state, respectively: they are schematically depicted in Figure 4B. A similar wetting behavior, called the frustrated complete wetting state, was found by one of the coauthors using hexane on water in the equilibrium condition.[30] To clarify the nature of these QL-droplet and QL-film on ice surfaces, we observe these in the various water vapor pressure conditions. When the pseudopartial wetting state was achieved (Figure 4C), the wetting angle of the QL-droplet on a bare ice surface (black/white arrowhead in Figure 4C) was 0.8°.[31] In contrast, when there were the QL-droplets only in the partial-wetting state

DOI: 10.1021/acs.accounts.8b00615
Acc. Chem. Res. 2019, 52, 1006−1015

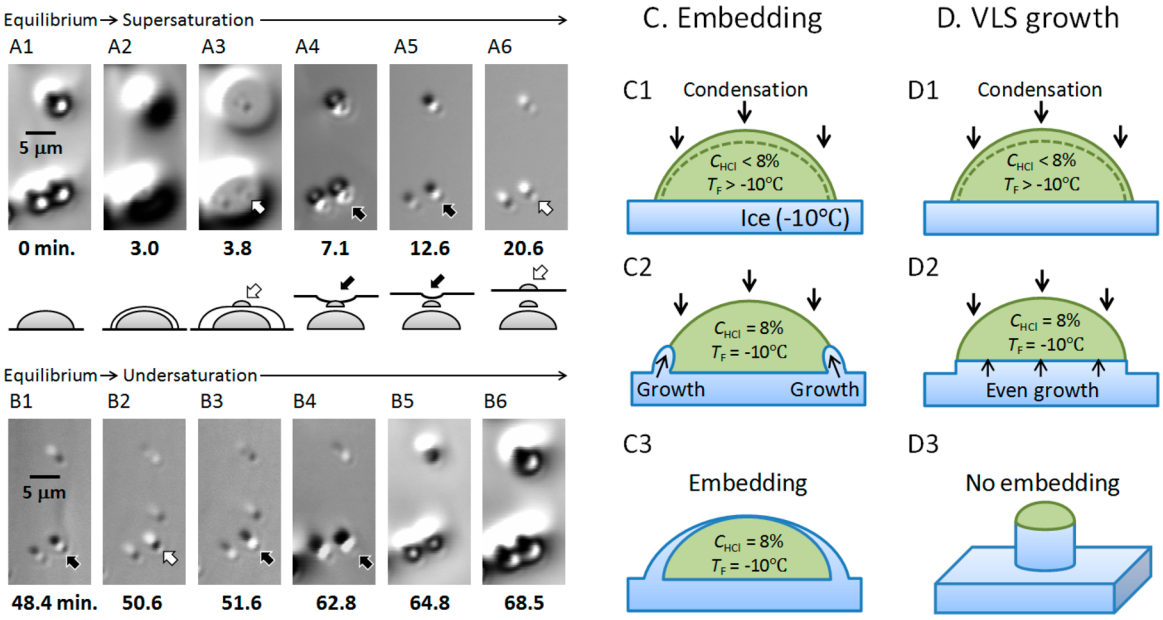

Figure 5. (A1–A6) Embedding and (B1–B6) reappearance of HCl droplets on an ice basal face at −10 °C observed by LCM-DIM. The white and black arrows show small HCl droplets and holes, respectively. (C) Embedding mechanism of HCl droplets in ice. (D) Conventional vapor–liquid–solid (VLS) growth mechanism. When the HCl concentration (C_{HCl}) in the droplets is 8 wt %, the freezing temperature (T_F) becomes −10 °C, and a part of the droplets start to freeze. Because the growth of ice preferentially starts from the droplet–ice–vapor interfaces (contact lines) (C1 and C2), the ice films finally cover the droplet surfaces (C3). However, if the ice–droplet interfaces grow evenly by VLS growth (D1 and D2), the droplets are not embedded in ice (D3). Reproduced with permission from ref 37. Copyright 2018 American Chemical Society.

(equivalent to the situation of the absence of the QL-droplet/QL-film in the pseudopartial-wetting state, Figure 4D), the wetting angle of the QL-droplet on a bare ice surface (black/white arrowhead in Figure 4D) was 2.3°. These indicate that the morphologies of the QL-droplet and QL-film can be linked to changes in their wettability. When the pseudopartial wetting state and the partial-wetting state coexist (Figure 4C), the QL-droplets on the QL-film (black arrowhead) and on the bare ice surface (black/white arrowhead) show very similar wetting angles (0.6° and 0.8°, respectively). This indicates that the QL-droplet experiences the wetting transition: with higher wettability of the QL-droplet on an ice surface, the wetting state changes from the partial wetting to the pseudopartial wetting.[31] Hence, we conclude that the QL-film and QL-droplet are in the same phase. However, since the QL-films are more strongly bound by ice crystal surfaces because of their smaller thickness (9 nm),[12] the QL-film shows higher viscosity than the QL-droplet.

Next, we discuss the behavior of the QL-film and QL-droplet states at different water vapor pressure and temperature conditions (Figure 4E).[31,32] In regions 1 and 2 of Figure 4E (supersaturated water vapor condition), the pseudopartial wetting state with the QL-droplet on the QL-film and the partial wetting state with the QL-droplet on the bare ice surface exist, respectively. Similarly, in regions 1′ and 2′ (undersaturated water vapor condition), the pseudopartial wetting state and the partial wetting state are present, respectively. These are summarized in Figure 4(F). In the supersaturated (undersaturated) condition, only above −2 °C, QL-droplet and QL-film are generated through condensation of vapor (sublimation of ice) on the ice surface. While the formation mechanism of the QL-film and QL-droplet in the undersaturated condition needs further investigation in the future, it is important to note the absence of QL-droplet and/or QL-film in the vicinity of the vapor-ice equilibrium curve (regions 3 and 3′). This indicates that QL-droplet and QL-film emerge only under nonequilibrium conditions above −2 °C and that such QL-droplet and QL-film are a metastable phase. Interestingly, the surface of ice and its own melt (QL-droplet and QL-film) show incomplete wetting, as Elbaum and co-workers partly reported for the first time.[27] We note that QL-droplet and QL-film differ from the droplet and film of hexane on the top of water interface, as the QL-droplet and QL-film are present only under nonequilibrium condition, while the droplet and film of hexane can be present under equilibrium condition.

Phenomena at the Ice Surface

What do these macroscopic and molecular insights imply for processes occurring on the surface of ice? In the following, we highlight two important aspects: interaction between atmospheric gas and ice surfaces and the slipperiness of ice.

Interaction with Atmospheric Gas. The uptake of trace gas species in snow and ice is a key process in atmospheric chemistry.[5] Among these, acidic gases (e.g., HCl) has been actively studied,[33] because these trigger heterogeneous chemical reactions that deplete the stratospheric ozone.[34,35] Understanding the behavior and dynamics of these gases on ice surfaces is of particular importance, as the adsorption rates and accommodation lifetime of these species are governed by their state of being. Nagashima and co-workers have recently carried out in situ LCM-DIM observations of single ice crystal surfaces by exposure to HCl gas at partial pressure (P_{HCl}) of 100 Pa.[36,37] As is seen in Figure 5A1, droplets with a 1–10 μm radius of HCl solution (8 wt %), which is thermodynamically stable below 0 °C, emerges on ice surfaces at T = −10 °C.

One can monitor the behavior of the HCl droplet during the growth and sublimation of ice crystals.[44] When the ice crystal is grown in supersaturated vapor, the HCl droplets are embedded in the ice crystals (Figure 5A). When the ice is subsequently

DOI: 10.1021/acs.accounts.8b00615
Acc. Chem. Res. 2019, 52, 1006–1015

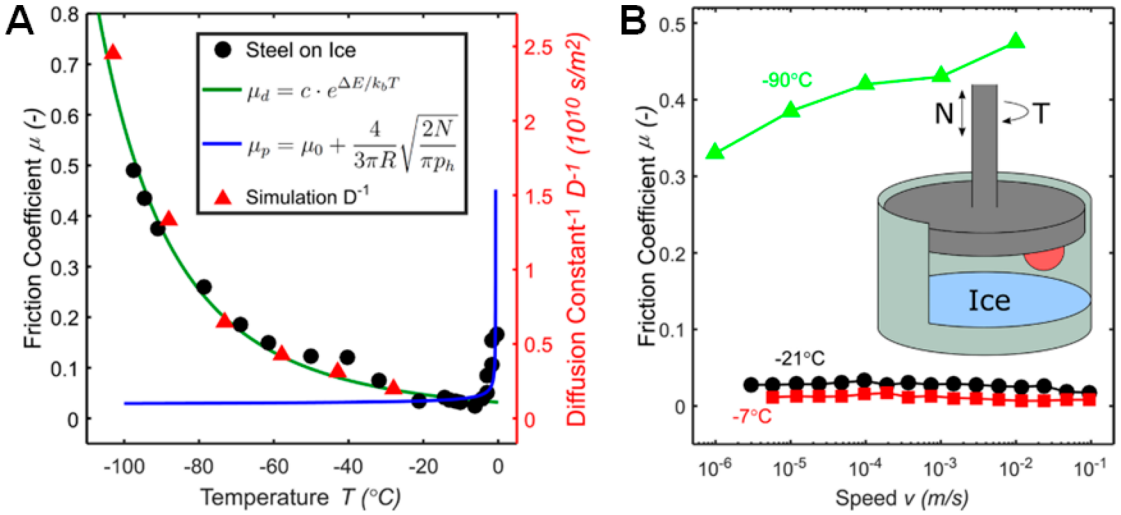

Figure 6. (A) Steel-on-ice friction coefficient vs temperature measured at a constant sliding speed of 0.38 mm s^{-1} (black circles), as well as the inverse diffusion constant (D^{-1}) of the DA water species at the topmost water layer of an ice surface as obtained from simulations. An Arrhenius fit (green line) and the prediction from plastic plowing through ice (blue line) are also plotted. (B) Friction coefficient of ice vs sliding speed of the steel ball. Reproduced with permission from ref 9. Copyright 2018 American Chemical Society.

sublimated in undersaturated vapor, the embedded HCl droplets reappear (Figure 5B). After the adequate sublimation of ice, the original HCl droplets recover (see Figure 5A1 and B6). Such embedding and reappearance could be observed irrespective of the degree of supersaturation/undersaturation adopted in the study. This HCl uptake mechanism cannot be explained by a conventional vapor−liquid−solid growth, where one can expect that the ice growth lifts up the HCl droplets (Figure 5C and D).[38] These results clearly demonstrate the breakdown of the homogeneous picture of the ice surface by acidic gas. Although the embedding of the HCl droplets suggests that the growth of ice starts from the droplet-ice-vapor interfaces (contact lines), a detailed molecular-level understanding on the growth is not yet clear. Input from simulation as well as further experimental probes are required for clarification.

The molar fraction of HCl included in the ice by the embedding of the HCl droplet is 0.19% at −15 °C. This value is 10 times larger than the solubility of HCl in an ice crystal (0.017%).[39] So far it has been thought that HCl gas is adsorbed and stored on ice crystal surfaces and that the contribution of bulk ice crystals to the HCl uptake is small. However, the embedding of the HCl droplets shows that the bulk ice crystals may play an important role in the uptake of HCl even in stratospheric conditions (e.g., T < −65 °C and P_{HCl} = 10^{-5} Pa). Uncovering the behavior of HCl droplets in such conditions is also a future challenge.

The Slipperiness of the Ice Surface. The slipperiness (or low friction coefficient) of ice surfaces has been attributed to the presence of QLL. However, it is not clear how such QLL can make the ice surface slippery. Here, we account for the mechanism of the slippery ice surface based on the molecular motion in the disordered topmost layer.

First, we consider the macroscopic friction coefficient of the ice as measured by varying temperature. These data are shown in Figure 6A. The friction coefficient changes drastically with temperature, and the friction coefficient shows a minimum at −7 °C. When the temperature increases above −7 °C, the ice friction increases. In this temperature range, the contact becomes fully plastic and the ice is irreversibly deformed, increasing the friction coefficient. The ice friction increases with decreasing temperature below −7 °C and reaches the coefficient of 0.5 at −90 °C. The coefficient of ∼0.5 is typically observed for solid-on-solid friction. We fit the ice friction coefficient below −7 °C using an Arrhenius fit (the green line in Figure 6A). The fit gives an activation barrier of ∼11 kJ/mol.

Such a large variation of the friction coefficient with temperature has been explained mainly by frictional melting.[40] However, Figure 6B reveals that the ice friction in fact is (nearly) insensitive to varying the sliding velocity by 4 orders of magnitude in the low-friction regime.[9] The observation of velocity-independent friction is inconsistent with the frictional melting hypothesis, since the sliding velocity controls the contact temperature.[41]

Here, we assign the ice friction to the microscopic dynamics of interfacial water molecules in the topmost disordered layer of ice. As shown above, a temperature increase induces the conversion of energetically stable DAA species to unstable DA species. This means that, on average, an interfacial water molecule with a free O−H group is increasingly likely to be a DA species at higher temperature, at the expense of DAA species. Increase in the number of unstable DA species allows the interfacial water molecules to exchange the hydrogen bond, enhancing the mobility of the interfacial DA water species. This is shown in Figure 6A, where the inverse diffusion constant (D^{-1}) of the interfacial DA water molecules is calculated from MD simulations. Interestingly, the activation barrier for the DA water molecule, calculated from plotting this inverse diffusion constant vs temperature is ∼11 kJ/mol, which amounts to half of the hydrogen bonding energy. This activation energy can be rationalized by the fact that the rotation of the DA species requires the hydrogen bond breaking and formation. Surprisingly, the activation energy of the diffusion constant of the interfacial DA water molecules is the same as the activation energy observed for the macroscopically measured ice friction coefficient.[9] These strongly suggest that the dynamics of the topmost interfacial water molecules play a central role in reducing the friction of ice surfaces.[9,10]

DOI: 10.1021/acs.accounts.8b00615
Acc. Chem. Res. 2019, 52, 1006−1015

Future Challenges

Above, we have outlined the different types of QL states on the top of the ice surface. The QL-droplet and QL-film emerging in the partial wetting and pseudopartial wetting conditions have been clearly observed using confocal microscopy, while these have not been well-investigated on the molecular-scale. For example, MD simulations have not been used to reproduce such droplet and film under nonequilibrium conditions, presumably due to the limited size of the system and length of the trajectory. Analogously, SFG has not been applied for probing the structure and dynamics of the QL-droplet and QL-film above −2 °C. Surface sensitive X-ray and neutron scattering techniques would also be highly required for a quantitative determination of the liquids pair correlation function. Thus, at present it is not clear how the microscopic structure of QL-droplet, QL-film, and disordered layer differ and how the disordered layer coexists with the QL-droplet and QL-films. Answering these questions is a challenge for MD simulations and SFG spectroscopy.

Similarly, the relationship between macroscopic and microscopic observations is still not well-understood. For example, the speed of the layer-by-layer growth of ice surfaces covered with the disordered layers shows a local maximum at ∼ −16 °C,[42] where the second bilayer has been observed to melt, as is discussed above. Connecting such a microscopic observation on the layer-by-layer melting with the macroscopic observation on the layer-by-layer growth of the disordered layers[29,42] is essential to reveal the nature of the disordered layer. The layer-by-layer growth of ice surfaces beneath the QL-film[43] will also provide a deeper insight into the nature of the QL-films. Furthermore, identifying the thickness of the disordered layer near the melting point is a future challenge. As is outlined above, the three different QL states can be present in the nonequilibrium condition, and to clarify the thickness of the disordered layer, one needs to control the vapor pressure very carefully to maintain the system under equilibrium conditions.

CONCLUSION

We have reviewed recent progress in experimental/simulation probing of QLL at the ice−air interface and presented a unified view on the different QL states based on equilibrium/nonequilibrium and temperature conditions. An important outcome is the disentanglement of the disordered layers formed under equilibrium conditions from the QL-droplets and the QL-films formed only under nonequilibrium conditions. The disordered layers consist of the topmost 2−3 water layers at the ice-air interface and arise from the lack of hydrogen-bond partners in the topmost water layer due to the presence of air. SFG spectroscopy combined with MD simulations reveals that the topmost layer of the ice surface is disordered at −90 °C, while the second layer is disordered at −16 °C. The disorder causes the conversion of the DAA to DA water species in the topmost ice layer. We demonstrate that this conversion appears to be crucial to account for the slipperiness of ice. Above −2 °C, LCM-DIM observation shows that the QL-droplets and the QL-films are kinetically formed and thus in a metastable state under the supersaturated or undersaturated vapor conditions. There is no such QL-droplet and QL-film in the conditions close to the vapor-ice equilibrium. We demonstrate that such QL-droplets bring a unique gas-uptake mechanism. Although we have disentangled the disordered layer from the QL-droplets and the QL-films, there is no MD simulation or experimental data to indicate the coexistence of the disordered layer and QL-droplet/QL-film. Addressing this question is a future challenge.

AUTHOR INFORMATION

Corresponding Authors

*E-mail: bonn@mpip-mainz.mpg.de.
*E-mail: sazaki@lowtem.hokudai.ac.jp.

ORCID

Yuki Nagata: 0000-0001-9727-6641
Tetsuya Hama: 0000-0002-4991-4044
Ellen H. G. Backus: 0000-0002-6202-0280
Markus Mezger: 0000-0001-9049-6983
Daniel Bonn: 0000-0001-8925-1997
Mischa Bonn: 0000-0001-6851-8453
Gen Sazaki: 0000-0002-2320-5442

Notes

The authors declare no competing financial interest.

Biographies

Yuki Nagata is a group leader at the Max Planck Institute for Polymer Research (MPI-P), Mainz, Germany. He received his PhD in 2007 from Kyoto University. After his stay at BASF SE and the University of California, Irvine, he joined MPI-P in 2011. His research focus is on the theoretical design of vibrational spectroscopy.

Tetsuya Hama is an assistant professor at the Institute of Low Temperature Science (ILTS) at Hokkaido University, Japan. He received his PhD in 2010 from Kyoto University, Japan. Subsequently, he joined ILTS. His research focuses on surface-reaction dynamics of molecules relevant to atmospheric chemistry and astrochemistry.

Ellen H. G. Backus is a group leader at MPI-P, Mainz, Germany, and a professor of physical chemistry at University of Vienna, Austria. She obtained her PhD in 2005 from Leiden University, The Netherlands. After postdoctoral research at the University of Zurich and AMOLF, she joined MPI-P in 2012. Her research focuses on the structure and dynamics of water at the molecular level at various interfaces.

Markus Mezger is a group leader at MPI-P and an assistant professor at the Institute of Physics, Johannes Gutenberg University Mainz, Germany. He received his PhD in 2008 from the University of Stuttgart. After postdoctoral research at the University of California, Berkeley, and at the Lawrence Berkeley National Lab, he joined MPI-P in 2010. His research focuses on the structure and dynamics of soft matter interfaces and in confinement studied by X-ray and neutron scattering techniques.

Daniel Bonn is a director of the van der Waals-Zeeman Institute of the University of Amsterdam, The Netherlands, where he obtained his PhD in 1993. Before returning to Amsterdam, he was a CNRS research director at the Ecole Normale Supérieure in Paris. He works on the nonlinear physics and hydrodynamics of complex fluids, focusing on phase transitions, glassy dynamics, and yield stress materials.

Mischa Bonn is a director at MPI-P, Mainz, Germany. He received his PhD in 1996 from the University of Eindhoven, The Netherlands. After postdoctoral research at the Fritz Haber Institute and Columbia University, he worked at Leiden University. In 2004 he became a group leader at AMOLF, Amsterdam, The Netherlands. In 2011 he joined MPI-P. His research interests are the structure and dynamics of molecules at interfaces and electron transfer across interfaces.

DOI: 10.1021/acs.accounts.8b00615
Acc. Chem. Res. 2019, 52, 1006−1015

Gen Sazaki is a full professor at ILTS, Hokkaido University, Japan. He received his PhD in 1994 from Osaka City University. After he became an assistant professor and a lecturer at Tohoku University, he joined ILTS in 2008. His research interests are crystal growth physics, structures and dynamics of surfaces/interfaces, and the development of advanced optical microscopy.

■ ACKNOWLEDGMENTS

We are grateful for financial support from the MaxWater Initiative from the Max Planck Society and from JSPS KAKENHI (Grant Numbers JP23246001 and JP15H02016).

■ REFERENCES

(1) Li, Y.; Somorjai, G. A. Surface Premelting of Ice. *J. Phys. Chem. C* **2007**, *111*, 9631−9637.
(2) Frenken, J. W. M.; van der Veen, J. Observation of Surface Melting. *Phys. Rev. Lett.* **1985**, *54*, 134−137.
(3) Rosenberg, R. Why Is Ice Slippery? *Phys. Today* **2005**, *58*, 50−55.
(4) Watanabe, N.; Kouchi, A. Ice Surface Reactions: A Key to Chemical Evolution in Space. *Prog. Surf. Sci.* **2008**, *83*, 439−489.
(5) Bartels-Rausch, T.; Jacobi, H. W.; Kahan, T. F.; Thomas, J. L.; Thomson, E. S.; Abbatt, J. P. D.; Ammann, M.; Blackford, J. R.; Bluhm, H.; Boxe, C.; Domine, F.; Frey, M. M.; Gladich, I.; Guzmán, M. I.; Heger, D.; Huthwelker, T.; Klán, P.; Kuhs, W. F.; Kuo, M. H.; Maus, S.; Moussa, S. G.; McNeill, V. F.; Newberg, J. T.; Pettersson, J. B. C.; Roeselová, M.; Sodeau, J. R. A Review of Air-Ice Chemical and Physical Interactions (AICI): Liquids, Quasi-Liquids, and Solids in Snow. *Atmos. Chem. Phys.* **2014**, *14*, 1587−1633.
(6) Petrenko, V. F.; Whitworth, R. W. *Physics of Ice*; Oxford University Press, 1988.
(7) Wei, X.; Miranda, P. B.; Shen, Y. R. Surface Vibrational Spectroscopic Study of Surface Melting of Ice. *Phys. Rev. Lett.* **2001**, *86*, 1554−1557.
(8) Wei, X.; Miranda, P. B.; Zhang, C.; Shen, Y. R. Sum-Frequency Spectroscopic Studies of Ice Interfaces. *Phys. Rev. B: Condens. Matter Mater. Phys.* **2002**, *66*, 085401.
(9) Weber, B.; Nagata, Y.; Ketzetzi, S.; Tang, F.; Smit, W. J.; Bakker, H. J.; Backus, E. H. G.; Bonn, M.; Bonn, D. Molecular Insight into the Slipperiness of Ice. *J. Phys. Chem. Lett.* **2018**, *9*, 2838−2842.
(10) Louden, P. B.; Gezelter, J. D. Why Is Ice Slippery? Simulations of Shear Viscosity of the Quasi- Liquid Layer on Ice. *J. Phys. Chem. Lett.* **2018**, *9*, 3686−3691.
(11) Sazaki, G.; Zepeda, S.; Nakatsubo, S.; Yokomine, M.; Furukawa, Y. Quasi-Liquid Layers on Ice Crystal Surfaces Are Made up of Two Different Phases. *Proc. Natl. Acad. Sci. U. S. A.* **2012**, *109*, 1052−1055.
(12) Murata, K. I.; Asakawa, H.; Nagashima, K.; Furukawa, Y.; Sazaki, G. In Situ Determination of Surface Tension-to-Shear Viscosity Ratio for Quasiliquid Layers on Ice Crystal Surfaces. *Phys. Rev. Lett.* **2015**, *115*, 256103.
(13) Asakawa, H.; Sazaki, G.; Nagashima, K.; Nakatsubo, S.; Furukawa, Y. Prism and Other High-Index Faces of Ice Crystals Exhibit Two Types of Quasi-Liquid Layers. *Cryst. Growth Des.* **2015**, *15*, 3339−3344.
(14) Nagata, Y.; Hasegawa, T.; Backus, E. H. G.; Usui, K.; Yoshimune, S.; Ohto, T.; Bonn, M. The Surface Roughness, but Not the Water Molecular Orientation Varies with Temperature at the Water−air Interface. *Phys. Chem. Chem. Phys.* **2015**, *17*, 23559−23564.
(15) Smit, W. J.; Tang, F.; Sánchez, M. A.; Backus, E. H. G.; Xu, L.; Hasegawa, T.; Bonn, M.; Bakker, H. J.; Nagata, Y. Excess Hydrogen Bond at the Ice-Vapor Interface around 200 K. *Phys. Rev. Lett.* **2017**, *119*, 133003.
(16) van der Veen, J. F. Melting and Freezing at Surfaces. *Surf. Sci.* **1999**, *433*−*435*, 1−11.
(17) Dash, J. G.; Rempel, A. W.; Wettlaufer, J. S. The Physics of Premelted Ice and Its Geophysical Consequences. *Rev. Mod. Phys.* **2006**, *78*, 695−741.
(18) Lipowsky, R.; Breuer, U.; Prince, K. C.; Bonzel, H. P. Multicomponent Order Parameter for Surface Melting. *Phys. Rev. Lett.* **1989**, *62*, 913−916.
(19) Li, H.; Bier, M.; Mars, J.; Weiss, H.; Dippel, A.-C.; Gutowski, O.; Honkimäki, V.; Mezger, M. Interfacial Premelting of Ice in Nano Composite Materials. *Phys. Chem. Chem. Phys.* **2019**, *21*, 3734−3741.
(20) Perakis, F.; De Marco, L.; Shalit, A.; Tang, F.; Kann, Z. R.; Kühne, T. D.; Torre, R.; Bonn, M.; Nagata, Y. Vibrational Spectroscopy and Dynamics of Water. *Chem. Rev.* **2016**, *116*, 7590−7607.
(21) Bonn, M.; Nagata, Y.; Backus, E. H. G. Molecular Structure and Dynamics of Water at the Water−Air Interface Studied with Surface-Specific Vibrational Spectroscopy. *Angew. Chem., Int. Ed.* **2015**, *54*, 5560−5576.
(22) Miyazaki, M.; Fujii, A.; Ebata, T.; Mikami, N. Infrared Spectroscopic Evidence for Protonated Water Clusters Forming Nanoscale Cages. *Science* **2004**, *304*, 1134−1137.
(23) Sánchez, M. A.; Kling, T.; Ishiyama, T.; van Zadel, M.-J.; Bisson, P. J.; Mezger, M.; Jochum, M. N.; Cyran, J. D.; Smit, W. J.; Bakker, H. J.; Shultz, M. J.; Morita, A.; Donadio, D.; Nagata, Y.; Bonn, M.; Backus, E. H. G. Experimental and Theoretical Evidence for Bilayer-by-Bilayer Surface Melting of Crystalline Ice. *Proc. Natl. Acad. Sci. U. S. A.* **2017**, *114*, 227−232.
(24) Qiu, Y.; Molinero, V. Why Is It So Difficult to Identify the Onset of Ice Premelting ? *J. Phys. Chem. Lett.* **2018**, *9*, 5179−5182.
(25) Pickering, I.; Paleico, M.; Sirkin, Y. A. P.; Scherlis, D. A.; Factorovich, M. H. Grand Canonical Investigation of the Quasi Liquid Layer of Ice : Is It Liquid? *J. Phys. Chem. B* **2018**, *122*, 4880−4890.
(26) Kling, T.; Kling, F.; Donadio, D. Structure and Dynamics of the Quasi-Liquid Layer at the Surface of Ice from Molecular Simulations. *J. Phys. Chem. C* **2018**, *122*, 24780−24787.
(27) Elbaum, M.; Lipson, S. G.; Dash, J. G. Optical Study of Surface Melting on Ice. *J. Cryst. Growth* **1993**, *129*, 491−505.
(28) Sazaki, G.; Matsui, T.; Tsukamoto, K.; Usami, N.; Ujihara, T.; Fujiwara, K.; Nakajima, K. In Situ Observation of Elementary Growth Steps on the Surface of Protein Crystals by Laser Confocal Microscopy. *J. Cryst. Growth* **2004**, *262*, 536−542.
(29) Sazaki, G.; Zepeda, S.; Nakatsubo, S.; Yokoyama, E.; Furukawa, Y. Elementary Steps at the Surface of Ice Crystals Visualized by Advanced Optical Microscopy. *Proc. Natl. Acad. Sci. U. S. A.* **2010**, *107*, 19702−19707.
(30) Shahidzadeh, N.; Bonn, D.; Ragil, K.; Broseta, D.; Meunier, J. Sequence of Two Wetting Transitions Induced by Tuning the Hamaker Constant. *Phys. Rev. Lett.* **1998**, *80*, 3992−3995.
(31) Murata, K.; Asakawa, H.; Nagashima, K.; Furukawa, Y.; Sazaki, G. Thermodynamic Origin of Surface Melting on Ice Crystals. *Proc. Natl. Acad. Sci. U. S. A.* **2016**, *113*, E6741−E6748.
(32) Asakawa, H.; Sazaki, G.; Nagashima, K.; Nakatsubo, S.; Furukawa, Y. Two Types of Quasi-Liquid Layers on Ice Crystals Are Formed Kinetically. *Proc. Natl. Acad. Sci. U. S. A.* **2016**, *113*, 1749−1753.
(33) Huthwelker, T.; Ammann, M.; Peter, T. The Uptake of Acidic Gases on Ice. *Chem. Rev.* **2006**, *106*, 1375.
(34) Finlayson-Pitts, B. J.; Pitts, J. N., Jr. *Chemistry of the Upper and Lower Atmosphere: Theory, Experiments, and Applications*; Academic Press: San Diego, CA, 2000.
(35) Abbatt, J. P. D.; Thomas, J. L.; Abrahamsson, K.; Boxe, C.; Granfors, A.; Jones, A. E.; King, M. D.; Saiz-Lopez, A.; Shepson, P. B.; Sodeau, J.; Toohey, D. W.; Toubin, C.; von Glasow, R.; Wren, S. N.; Yang, X. Halogen Activation via Interactions with Environmental Ice and Snow in the Polar Lower Troposphere and Other Regions. *Atmos. Chem. Phys.* **2012**, *12*, 6237−6271.
(36) Nagashima, K.; Sazaki, G.; Hama, T.; Asakawa, H.; Murata, K. I.; Furukawa, Y. Direct Visualization of Quasi-Liquid Layers on Ice

DOI: 10.1021/acs.accounts.8b00615
Acc. Chem. Res. 2019, 52, 1006−1015

Crystal Surfaces Induced by Hydrogen Chloride Gas. *Cryst. Growth Des.* **2016**, *16*, 2225−2230.
(37) Nagashima, K.; Sazaki, G.; Hama, T.; Murata, K.; Furukawa, Y. Uptake Mechanism of Atmospheric Hydrogen Chloride Gas in Ice Crystals via Hydrochloric Acid Droplets. *Cryst. Growth Des.* **2018**, *18*, 4117−4122.
(38) Wagner, R. S.; Ellis, W. C. Vapor-Liquid-Solid Mechanism of Single Crystal Growth. *Appl. Phys. Lett.* **1964**, *4*, 89−90.
(39) Thibert, E.; Dominé, F. Thermodynamics and Kinetics of the Solid Solution of HCl in Ice. *J. Phys. Chem. B* **1997**, *101*, 3554−3565.
(40) Kietzig, A. M.; Hatzikiriakos, S. G.; Englezos, P. Physics of Ice Friction. *J. Appl. Phys.* **2010**, *107*, 081101.
(41) Persson, B. N. J. Ice Friction: Role of Non-Uniform Frictional Heating and Ice Premelting. *J. Chem. Phys.* **2015**, *143*, 224701.
(42) Inomata, M.; Murata, K.; Asakawa, H.; Nagashima, K.; Nakatsubo, S.; Furukawa, Y.; Sazaki, G. Temperature Dependence of the Growth Kinetics of Elementary Spiral Steps on Ice Basal Faces Grown from Water Vapor. *Cryst. Growth Des.* **2018**, *18*, 786−793.
(43) Murata, K.; Nagashima, K.; Sazaki, G. How Do Ice Crystals Grow inside Quasi Liquid Layers? *Phys. Rev. Lett.* **2019**, *122*, 026102.
(44) Jambon-Puillet, E.; Shahidzadeh, N.; Bonn, D. Singular Sublimation of Ice and Snow Crystals. *Nat. Commun.* **2018**, *9*, 4191.
(45) Slater, B.; Michaelides, A. Surface Premelting of Water Ice. *Nature Rev. Chem.* **2019**, *3*, 172−188.

DOI: 10.1021/acs.accounts.8b00615
Acc. Chem. Res. 2019, 52, 1006−1015